Optimal Cable Laying Across an Earthquake Fault Line Considering Elliptical Failures

Cong Cao, Zengfu Wang, Moshe Zukerman, *Fellow, IEEE*, Jonathan Manton, *Senior Member, IEEE*, Alain Bensoussan, *Fellow, IEEE*, Yu Wang

***Abstract*—Whether it be a road, railway track, pipeline or fibre-optic cable, achieving a low probability of "cable" damage is important for the proper operation of modern infrastructure. This paper considers the fundamental problem of how to connect two points with a cable that crosses an earthquake fault line. We first develop a model, under certain general assumptions, for the cable break probability. Then we formulate a multi-objective optimization problem, with cable cost and probability of cable break being the two objectives. For two important and meaningful sets of cable shape alternatives, the Pareto front is determined for these two objectives. All the analytical results are verified by simulations.**

***Index Terms*—Cabling, cost minimization, earthquake, disaster, survivability, probability, pipeline, infrastructure.**

ACRONYMS AND ABBREVIATIONS:

CBP	Cable Break Probability
CCB	Conditional Cable Break
CSP	Cable Survival Probability
EFL	Earthquake Fault Line
HRA	Hook with Right Angles
TCS	Three Connected Segments

NOTATIONS:

$S = (x_S, y_S)$	a point S in $\mathbb{R}^2$ with coordinates (x_S, y_S). Points in $\mathbb{R}^2$ are denoted by uppercase letters, while the coordinates of such points are denoted by lowercase letters.
A, B	two endpoints of the EFL
$\mathcal{D}$	set of points on the EFL
$\hat{\mathcal{D}}$	length of the EFL
N_1, N_2	two points to be connected
e_1, e_2	coefficients of the linear function that describes the straight line $\overleftrightarrow{N_1N_2}$
$\hat{d}$	distance between N_1 and N_2
$\mathcal{L}$	set of points on the cable
c	cable cost per unit length
C	cost of the cable
e	eccentricity of the elliptical isoseismals
ε	$\sqrt{1-e^2}$
$d(M, S)$	equivalent distance from S to M
$d(S)$	equivalent distance from S to the cable
$P(\text{break})$	CBP function
λ	a parameter used in the numerical examples representing the exponential decay rate of the conditional cable break probability
$\overleftrightarrow{S_1S_2}$	line that contains S_1 and S_2
$\overline{S_1S_2}$	line segment between S_1 and S_2
$\mid S_1S_2 \mid$	length of $\overline{S_1S_2}$
Δ_T	length of middle segment of a TCS cable
Δ_H	length of last segment of a HRA cable
$d_1(S)$ – $d_3(S)$	three candidates for $d(S)$ under the straight line cable shape
$d_{T1}(S)$ – $d_{T5}(S)$	five candidates for $d(S)$ under TCS
$d_{H1}(S)$ – $d_{H3}(S)$	three candidates for $d(S)$ under HRA

The work described in this paper was supported by a grant from the Research Grants Council of the Hong Kong Special Administrative Region, China (Project No. CityU8/CRF/13G).

C. Cao and M. Zukerman are with the Department of Electronic Engineering, City University of Hong Kong, Kowloon, Hong Kong SAR, PRC (email: congcao2-c@my.cityu.edu.hk; m.zu@cityu.edu.hk).

Z. Wang is with the School of Automation, Northwestern Polytechnical University, Xi'an, PRC, and the Department of Electronic Engineering, City University of Hong Kong, Kowloon, Hong Kong SAR, PRC. (email: wangzengfu@gmail.com)

J. Manton is with the Department of Electrical and Electronic Engineering, The University of Melbourne, Victoria 3010, Australia (email: j.manton@ieee.org).

A. Bensoussan is with the Jindal School of Management, University of Texas at Dallas, Texas, USA, and the Department of Systems Engineering and Engineering Management (SEEM), City University of Hong Kong, Kowloon, Hong Kong SAR, PRC (email: abensous@cityu.edu.hk).

Y. Wang is with the Department of Architecture and Civil Engineering, City University of Hong Kong, Kowloon, Hong Kong SAR, PRC (email: yuwang@cityu.edu.hk).

I. INTRODUCTION

IN many applications, engineers are faced with a challenge of how to lay an optical fibre cable, a fuel or gas pipeline, electric power line, road or railway track between two points across an earthquake fault zone. Connecting the two points by a straight line will minimize cost but may increase the risk of damage or break in a case of an earthquake. In practice, engineers lay cables using a software package e.g.

MakaiPlan [1] and may consider potential earthquake hazards by introducing ad hoc adjustments. In this paper, we develop mathematical expressions and related numerical results for cable cost and risk of break that will provide new insights into how to lay a single cable between two points across an Earthquake Fault Line (EFL) assuming that earthquake epicenters only occur on the EFL.

Modern infrastructures have been adversely affected by a series of earthquakes with grave and costly consequences over the last century. Several examples of such earthquakes follow. In 1971, an earthquake in San Fernando caused about 1,400 breaks in various piping systems, which resulted in temporal disruption of water, gas and sewage services of the city [2]. In 1987, an earthquake in Colombia-Ecuador border region destroyed or badly damaged about 27 km of the oil pipeline in Ecuador, which may represented the largest single pipeline loss in history [3]. An earthquake of 7.1-magnitude on 26th December 2006 just south of Taiwan caused unprecedented damage to seven submarine communication cables. This incident caused severe disruption of Internet and phone services in south east Asia for several weeks [4]. Similar multiple-cable breaks happened twice in the Mediterranean sea in 2008, where the undersea cables connecting Europe, North Africa and Asia are concentrated in a small area [5]. A massive earthquake of 9.0-magnitude followed by a tsunami occurred near the east coast of Honshu, Japan on 11th March 2011, which destroyed or damaged at least 2,126 roads and 26 railways [6]. Many other strong and destructive earthquakes have occurred in the past and are likely to occur in the future.

There have been many research publications aiming to understand the effect of earthquakes and improve the survivability of modern infrastructures [7], [8]. Several researchers have studied certain past earthquakes to evaluate their potential damage on current infrastructures. For example, [9] evaluated the seismic risk of the water supply pipeline system in Los Angeles. [10], [11] investigated the potential damage to current natural gas or water pipelines in Taichung City, Taiwan from the 1999 Chi-Chi earthquake (also called Ji-Ji earthquake). Other researchers have focused on modeling and analyses of the vulnerability of infrastructure systems. The work presented in [12] considered power and gas pipeline systems, and proposed a methodological framework for analyzing the vulnerability of interdependent infrastructure systems. There is a method based on the identification of the parameters developed in [13] to assess the seismic vulnerability of water pipeline network. The study presented in [14] developed a Geographic Information Systems based probabilistic reliability model to assess seismic vulnerability of European gas and electricity networks in terms of various performance measures.

It is hard to develop a realistic disaster model, since disaster can happen anytime anywhere and the level of impact can vary as well [15]. Therefore, many researchers use computational geometric methods to model disasters and evaluate network resilience [16], [17]. For example, [18], [19] proposed a grid partition-based scheme to assess the network vulnerability under random region failures. In [20], the effects of disasters were considered as random line-cuts. The works presented in [21]–[24] attempted to identify the vulnerable points in geographic networks by finding the location of the worst-case failure (a line or disk cut) using certain network connectivity measures. In the research presented in [25]–[28], it was assumed that a disaster occurs as a randomly placed circular disk of a particular radius. This is known as the *circular disk failure model*. In [29], [30], circular disk failures were also considered in small networks to solve a problem of cost minimization subject to meeting a survival probability constraint.

Although the circular disk failure model [25]–[30] is popular, its generalization, the elliptical failure model is more suitable for many especially strong earthquakes. The elliptical failure model properly incorporates the direction dependent effects of earthquakes. Observations from many past earthquakes, such as the Charlevoix-Kamouraska earthquake (1925) [31], New Zealand earthquake (1929) [32], the Koyna earthquake (1967) [33], the Tonghai earthquake (1970) [34], the Tangshan earthquake (1976) [35], and the Kocaeli earthquake (1999) [36], have shown that the earthquake effects are indeed direction dependent and the shape of the isoseismals is elliptical. Note that, although an earthquake epicenter is frequently visualized as a point, the fault rupture inside the Earth's crust that causes the earthquake, in fact, occurs along a 3D plane and often propagates as an intermittent series of fault ruptures or slips within the ruptured zone. Along the parallel direction of fault ruptures, the earthquake effect tends to accumulate and becomes growingly significant as the intermittent series of fault ruptures occurs and propagates. In contrast, along the normal direction of fault ruptures, the accumulation of earthquake effect is less significant. This fault rupture mechanism leads to the common observation of elliptical isoseismals in many past earthquakes [37]. When the earthquake magnitude is small, the fault rupture zone is small and the earthquake epicenter may be well approximated as a point (i.e., no intermittent series of fault ruptures, but just a single event of fault rupture at a point). Therefore, the direction dependent effect is not significant and the elliptical isoseismals gradually converge to circular isoseismals [37]. When developing a general earthquake effect model without reference to specific fault systems or specific sites, an elliptical failure model is able to properly capture the direction-dependent effects of earthquakes. Clearly, the circular disk failure is a special case of the elliptical failure when the eccentricity of the ellipse is equal to 0, and therefore, all the results of this paper are also applicable to the circular disk failure model used in [25]–[30].

In addition to the elliptical failure assumption, we also assume that the conditional probability of a cable break (for a given epicenter) is a generally decaying function of a certain measure of the cable position and the location of the epicenter.

In addition to the above mentioned publications, there were many others (e.g. [38]–[47] and references therein) that have studied network survivability subject to one or more link or node failures. However, not many publications have focused on minimizing the risk of an individual link or cable failure.

This is the topic of the present paper.

There are many pairs of cities in the world that are directly connected by at least one cable that crosses at least one earthquake fault. Examples include: Lanzhou and Chengdu, San Jose and Los Angeles [48]–[50], etc.

The unique feature of this work is that we aim to optimize the shape of the single cable and to derive convenient expressions obtained by probabilistic analysis. This has not been done by any of the previous publications. We note that in [29], [30] certain cable shape scenarios have been considered for multiple cables between two nodes, but the results of [29], [30] are not applicable to the case we consider here of laying a single cable. In many cases, infrastructure vendors focus on the problem of laying a single cable and it is therefore an important problem on its own. A key performance measure in this paper is the cable break probability (CBP). It represents the probability that a cable breaks following an earthquake. A related concept is the cable survival probability (CSP), which is one minus the CBP. Meeting cable survivability requirement is an important design objective in addition to cost. We consider the problem of how to minimize the cost of laying a cable across an EFL, to maintain a required cable survivability probability in an earthquake event, or to minimize the CBP for a given budget. To this end, we formulate it as a multi-objective optimization problem that considers cable cost and CBP as the two objectives. We consider two important and meaningful sets of cable shape alternatives, and provide Pareto fronts for the two objectives. For tractability, to be able to obtain convenient expressions for determining the Pareto fronts, we rely on simplifications of a far more complex real world problem. Nevertheless, our solutions provide certain insight and useful guidance for cable laying. Furthermore, although the work here is written in the context of cabling, it has many other applications, including designs of fuel or gas pipelines, roads, railway tracks and power lines.

The remainder of the paper is organized as follows. In Section II, we describe the problem. In Section III, we provide a brief description and intuitive justification of the cable shape alternatives. In Section IV, we consider the cases of straight-line cables which provide insight into how to lay cables with low CBP. In Sections V and VI, we study two important alternatives of cable shapes and obtain expressions for the cost and CBP. After establishing the relevant monotonicity properties of the convenient probabilistic expressions, we provide Pareto fronts for cost and survival probabilities of the two alternatives. The paper is concluded in Section VII.

II. Preliminaries and Problem Description

As discussed, we consider tradeoff between the two objectives: cable cost and CBP. To obtain the Pareto front for these two objectives, we will provide proofs for their monotonicity. Having the Pareto front enables us to solve two single-objective optimization problems of minimizing cost subject to a constraint on the CBP, and minimizing CBP subject to a constraint on the cable cost, in a case of an earthquake.

The problem is defined in a 2-dimensional Euclidean space $\mathbb{R}^2$. We assume that only one destructive earthquake occurs at one time. This is justified by the low frequency of earthquakes and by the relatively short time cables are being repaired. Let $\mathcal{D} \subset \mathbb{R}^2$ be a set of points on the EFL where an earthquake epicenter may occur. A coordinate system is constructed so that the origin is at the midpoint between the two endpoints of the EFL: A and B. We assume for simplicity that the set $\mathcal{D}$ is a segment of a straight line $y = 0$. Let $\hat{\mathcal{D}}$ be the length of the EFL. Thus A and B are positioned at the x-axis points $(-\hat{\mathcal{D}}/2, 0)$ and $(\hat{\mathcal{D}}/2, 0)$, respectively.

Let N_1 and N_2 be the two points to be connected with a cable. Let e_1, e_2 denote the slope and the intercept of the straight line $\overleftrightarrow{N_1N_2}$. The coordinates of N_1 and N_2 are (x_{N_1}, y_{N_1}) and (x_{N_2}, y_{N_2}), where $x_{N_1} < x_{N_2}$, $y_{N_1} = e_1 x_{N_1} + e_2$ and $y_{N_2} = e_1 x_{N_2} + e_2$. The distance between N_1 and N_2 is

$$\hat{d} = |x_{N_2} - x_{N_1}|\sqrt{1 + e_1^2}.$$

A cable is defined as a continuous curve that connects N_1 and N_2 in $\mathbb{R}^2$. Let $\mathcal{L}$ be the set of points on the cable. Let $\hat{\mathcal{L}}$ be the length of the cable and C be the cost of the cable. The cable cost is assumed to be a linear function of its length. Thus, $C = c\hat{\mathcal{L}}$, where c is the cost per unit length.

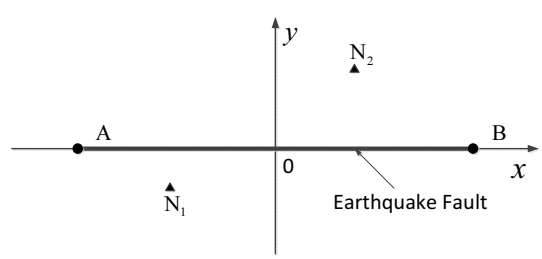

Fig. 1. The locations of the two points and the EFL.

We further assume that

$$\begin{aligned} -\frac{\hat{\mathcal{D}}}{2} < \frac{e_2}{e_1} < \frac{\hat{\mathcal{D}}}{2}, \\ y_{N_1} y_{N_2} < 0, \\ \hat{\mathcal{D}} \gg \hat{d}. \end{aligned} \tag{1}$$

These assumptions are made to ensure that the two points of the cable are located on each side of the EFL, and the length of the EFL is sufficiently longer than the distance between the two points so that laying a cable between the two points without crossing the fault line is too costly to be considered as the optimal solution. This is a reasonable assumption because the length of some earthquake faults is many hundreds of kilometers and crossing them is unavoidable. An example of the EFL and the two points is illustrated in Fig. 1.

In this paper, we assume that the distribution of an earthquake effect is described by a series of concentric elliptical isoseismals, whose major axes are on the EFL. They have a common eccentricity denoted by e, which is assumed to be fixed for every possible epicenter on the EFL. Therefore, throughout the paper, all the ellipses we analyze and discuss

share a common eccentricity e. The equation of an ellipse given that an epicenter occurs at S is

$$\frac{(x - x_S)^2}{a^2} + \frac{y^2}{b^2} = 1,$$

where a and b are the semi-major axis and semi-minor axis, and $b^2 = (1 - e^2)a^2 = \varepsilon^2 a^2$. For historical earthquake events, the author of [51] proposed a method of drawing an individual elliptical isoseismal to enclose all observations of a particular intensity or ground motion measure through regression analysis. Then the semi-axes a, b and the eccentricity e can be obtained by the derived elliptical isoseismal. Fig. 2 illustrates an earthquake with elliptical isoseismals. For every point on an isolated isoseismal, the earthquake effect is same.

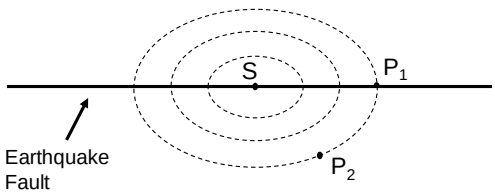

Fig. 2. A visual description of an elliptical earthquake.

For any point $S \in \mathcal{D}$ and a point $M \in \mathbb{R}^2$, we define the *equivalent distance* from S to M as follows.

$$d(M, S) = \sqrt{(M - S)^T Q (M - S)}, \tag{2}$$

where $Q = \begin{bmatrix} 1 & 0 \\ 0 & 1/\varepsilon^2 \end{bmatrix}$. In fact, the equivalent distance $d(M, S)$ is the length of the semi-major axis of the elliptical isoseismal (whose epicenter is S and eccentricity is e) on which the point M is located. In Fig. 2, P_1 and P_2 share the same equivalent distance to S which is $|SP_1|$. Furthermore, the equivalent distance from S to the cable is defined as

$$d(S) = \min_{M \in \mathcal{L}} d(M, S), \tag{3}$$

i.e., $d(S)$ is equal to the length of the shortest semi-major axis of the ellipses (whose epicenter is S and eccentricity is e) that intersect with the cable. Because strong motions and effects of an earthquake tend to attenuate as the distance increases between the earthquake epicenter and the locations considered, we assume that all points on a given ellipse have the same earthquake effect on the cable, and that a point closer to the epicenter in terms of the equivalent distance than another implies stronger motions and higher cable break probability. Therefore, the shorter the equivalent distance is from the epicenter to the cable, the more likely the cable is to break in a case of an earthquake. Accordingly, we assume that the conditional cable break (CCB) probability function, given that an earthquake epicenter occurs at S and the eccentricity of the elliptical isoseismals is e, is a monotonically decreasing derivable function of $d(S)$, and denoted by,

$$P(\text{break} \mid S) = q(d(S)).$$

Throughout the paper, we use $q(\cdot)$ as a generalized CCB function to derive convenient expressions obtained by probabilistic analysis. Let $p(S)$ be the continuous probability density function of an earthquake epicenter occurring at S on $\mathcal{D}$. The CBP is therefore given by

$$P(\text{break}) = \int_{S \in \mathcal{D}} P(\text{break} \mid S) p(S) dS. \tag{4}$$

Remark. *In cases where we know the location of the fault line but we have very limited information on the geology and the history of earthquakes and ground motion, then it is appropriate to assume an earthquake epicenter is uniformly distributed on the EFL [52], [53], i.e., $p(S)$ is a uniform distribution probability density function. However, in cases where extensive information is available, e.g. by USGS in California [54], more accurate prediction on the location of the epicenter may be made using other distributions. The results in the paper are not limited to a specific probability density function of epicenter's location. In addition, any non-negative decreasing derivable function can be used as the CCB function $q(\cdot)$, although we will adopt exponential decay function as an example in the numerical illustration later.*

III. Description and Intuitive Justification of the Cable Shape Alternatives

The straight line is the least cost option of laying the cable. The insight that will be gained from Section IV points out to the benefit of positioning the cable vertically to the EFL which intuitively reduces the length of the cable in the "danger zone" that may be affected by an earthquake. The term "danger zone" is loosely defined to mean the area close to the EFL where the probability of cable break is significant. Note that the earthquake epicenter can occur anywhere on the EFL and cable breaks occur according to the model we have described. If the CCB function is characterized by, for example, an exponential distribution, and the probability density function of the earthquake epicenter is characterized by uniform distribution, then it is difficult to assess where exactly the probability of cable break is "significant" and where it is not. Despite the fact that the "danger zone" definition is somewhat loose, it is appropriate for intuitive explanations.

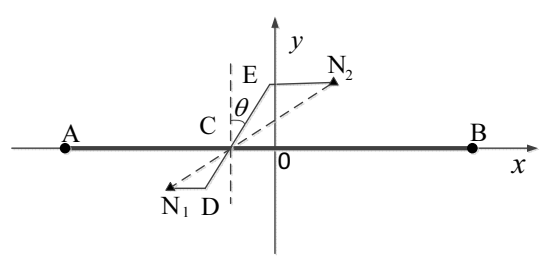

Fig. 3. A visual description of TCS.

Generally speaking, and ignoring third dimensional considerations such as the earth curvature or the topography, laying a cable in a straight line or in a sequence of a few straight line segments is a common industry practice [55]. Observing the map in [56], for example, it is clear that the shape of

cables, even if they are of length of thousands of kilometers, is a sequence of few straight lines. When there is no risk or third dimensional considerations, laying a cable in a straight line is cheaper and simpler. Accordingly, in our case, no more than three straight line segments are considered between N_1 and N_2: two lines that one of their endpoints is either N_1 and N_2 and a third line that connects these two lines and crosses the EFL through the "danger zone". We call such a cable shape that comprises three segments: Three Connected Segments (TCS). Based on the insight that will be gained from Section IV, having the middle segment vertical to the EFL will give the lowest risk in terms of CBP and this is indeed the option used in practice by cable surveyors [55]. On the other hand, a straight line between N_1 and N_2 will give the lowest cost. Accordingly, the TCS provides a wide range of practical cable shape alternatives for which tradeoffs between cost and risk can be assessed.

In Section V, we derive expressions for the CBP and cost for a TCS cable shape as a function of the length and the slope of the middle cable segment. From these expressions we can derive the Pareto front for the two objectives by varying the length and the slope of the middle segment, after we establish the monotonicity of the CBP and cable cost function.

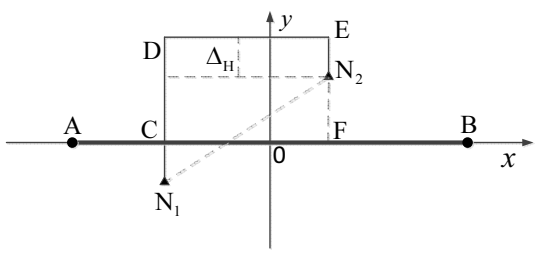

Fig. 4. A visual description of HRA.

Further significant CBP reduction, for an additional cable length cost, can be achieved by Hook with Right Angle (HRA), where we position a segment of cable parallel to the EFL and use two vertical segments to connect it to the two endpoints. Both the benefit in CBP reduction and the cable cost depends on the distance between the parallel segment and the EFL. Therefore, we vary in Section VI this distance and study its effect on cost and risk. HRA is especially applicable to the cases where the endpoints are located far from each other but their distance to the EFL is not too far. Consider the limit where their distance to the EFL is fixed, but the distance between the endpoints is arbitrarily large. Under such a limit, it is clear that the main part of the cable under HRA is the segment that is parallel to the EFL. HRA keeps the cable parallel to the EFL for a sufficiently long distance. In the limit, the cost of HRA approaches the cost of the straight line but if the distance of the parallel segment from the EFL is far enough (this has negligible cost implication in this case), HRA can achieve very low risk of cable break. Generally, HRA has lower risks than TCS which is demonstrated numerically in Section VI. The two sets (TCS and HRA) of cable alternatives cover a wide range of CBP variations from the least cost straight line case to the low risk case of HRA.

IV. Straight Line Cable

In this section we only consider cases where the two points are connected by a single cable in a straight line. First we derive the CBP of such a cable, and then, we consider various angles between the cable and the EFL to study their effect on CBP.

A. Line segment between N_1 and N_2

Without loss of generality, we assume that the slope of $\overline{N_1N_2}$ is greater than 0. We further assume, without loss of generality, that N_1 is closer to the EFL than N_2. Thus, we have $e_1 > 0$ and $|y_{N_1}| < |y_{N_2}|$.

The straight line segment between N_1 and N_2 has important applications throughout the paper. The assumptions we have made above, that are without loss of generality, are also relevant to the various analyzes in Sections V and VI.

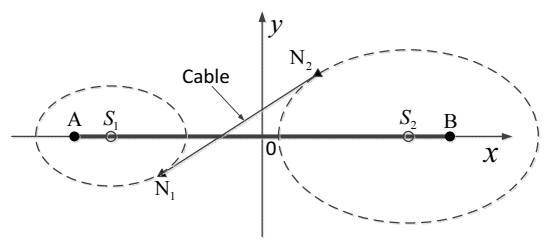

Fig. 5. A visual description of the problem with straight line shape cable

We restrict the cable function to be $y = e_1x + e_2$, where $x_{N_1} \le x \le x_{N_2}$, as shown in Fig. 5. Therefore, for any point $S = (x, 0)$ on the EFL, we have

$$\begin{aligned} d(S) &= \min_{M\in\mathcal{L}} d(M,S) \\ &= \min_{M\in\mathcal{L}} \sqrt{(x_M - x)^2 + (e_1x_M + e_2)^2/\varepsilon^2}. \end{aligned} \tag{5}$$

Hereinafter, we will use interchangeably the notation $d(S)$ and $d(x)$ for the equivalent distance from S to the cable. Let the derivative of $d(M,S)$ (of the variable x_M) be 0, then we obtain

$$x = x_M + e_1(e_1x_M + e_2)/\varepsilon^2 = x_M + e_1y_M/\varepsilon^2.$$

Since we have $x_{N_1} \le x_M \le x_{N_2}$, let $x_{S_1} = x_{N_1} + e_1y_{N_1}/\varepsilon^2$ and $x_{S_2} = x_{N_2} + e_1y_{N_2}/\varepsilon^2$. Here S_1, S_2 are the epicenters of the two ellipses (whose eccentricity is e) such that $\overline{N_1N_2}$ is the tangent at N_1 and N_2 to the two ellipses respectively, as shown in Fig. 5. According to value of x, there are three candidates of $d(S)$, which are

$$\begin{aligned} d_1(x) &= \sqrt{(x_{N_1} - x)^2 + y_{N_1}^2/\varepsilon^2}, && x \le x_{S_1}, \\ d_2(x) &= \frac{|\, e_1x + e_2 \,|}{\sqrt{e_1^2 + \varepsilon^2}}, && x_{S_1} < x < x_{S_2}, \\ d_3(x) &= \sqrt{(x_{N_2} - x)^2 + y_{N_2}^2/\varepsilon^2}, && x \ge x_{S_2}. \end{aligned} \tag{6}$$

The three candidates for $d(S)$ have the following geometric meanings:

1) $d_1(x)$: the equivalent distance from S to N_1;
2) $d_2(x)$: the equivalent distance from S to $\overleftrightarrow{N_1N_2}$;
3) $d_3(x)$: the equivalent distance from S to N_2.

Then, the CBP (with the assumptions $x_A < x_{S_1}$ and $x_B > x_{S_2}$) is obtained by

$$\begin{aligned} &P(\text{break}) \\ &= \int_{-\hat{\mathcal{D}}/2}^{x_{N_1}+e_1 y_{N_1}/\varepsilon^2} q\left(\sqrt{(x_{N_1}-x)^2+y_{N_1}^2/\varepsilon^2}\right) p(x)dx \\ &+ \int_{x_{N_1}+e_1 y_{N_1}/\varepsilon^2}^{x_{N_2}+e_1 y_{N_2}/\varepsilon^2} q\left(\frac{\mid e_1 x + e_2 \mid}{\sqrt{e_1^2+\varepsilon^2}}\right) p(x)dx \\ &+ \int_{x_{N_2}+e_1 y_{N_2}/\varepsilon^2}^{\hat{\mathcal{D}}/2} q\left(\sqrt{(x_{N_2}-x)^2+y_{N_2}^2/\varepsilon^2}\right) p(x)dx. \end{aligned}$$

To illustrate the CBP in a numerical example, an explicit CCB function is required. In seismology, exponential distributions are commonly used for seismic hazard assessments [57]–[59]. Hence, in our numerical examples, for simplicity of exposition and without loss of generality, we consider a negative exponential function as the CCB function and a uniformly distributed probability density function for epicenters to obtain numerical results, which are

$$P(\text{break} \mid S) = q(d(S)) = e^{-\lambda d(S)}, \quad p(S) = \frac{1}{\hat{\mathcal{D}}}, \tag{7}$$

where λ is a given parameter representing the exponential decay rate of the conditional cable break probability. The parameter λ may be estimated from repair records of buried utilities during past earthquakes. For example, the 1994 Northridge earthquake in Los Angeles caused substantial damage to the water distribution system in Los Angeles. The water trunk line (nominal pipe diameter $\geq$ 600mm) were damaged at 74 locations (e.g., [9]), and water distribution pipelines (nominal pipe diameter $<$ 600mm) were repaired at 1013 locations (e.g., [60]). Using these repair records, Jeon and O'Rourke [60] have developed correlations between pipeline repair rate (repairs/km) and peak ground velocity (PGV) for pipelines with different types of material. Understanding of the relationship between PGV and repair rate can lead to approximations of the (decreasing) CCB function and in the particular case of the exponential function to the estimation of λ in the area under consideration. For the example based on the parameters described in Table I, the CBP is 0.3379 and the cable cost is 492.7038.

TABLE I
PARAMETERS USED FOR THE NUMERICAL RESULTS.

(x_{N_1}, y_{N_1})	(x_{N_2}, y_{N_2})	e	λ	e_1	e_2	$\hat{\mathcal{D}}$	c
$(-216, -27)$	$(270, 54)$	$\frac{2}{3}$	$\frac{1}{54}$	$\frac{1}{6}$	9	1080	1

B. Rotated straight line cable around N_1

Let the angle between the EFL and the straight line cable be α, see Fig. 6. Here we rotate the straight line cable around N_1

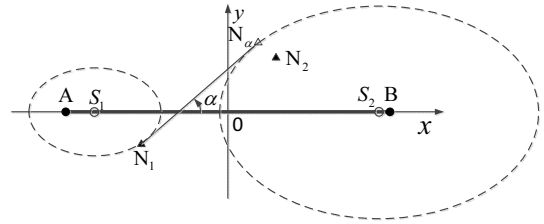

Fig. 6. The rotation of the straight line cable

to observe how α affects CBP. We fix N_1 and keep the cable length unchanged. We rotate the cable around N_1 and increase the angle α until $\alpha = 90°$. The new endpoint of the cable is denoted by N_α. We redefine $d_2(S)$ as the equivalent distance from S to $\overleftrightarrow{N_1N_\alpha}$ and redefine $d_3(S)$ as the equivalent distance from S to N_α. Let a be the slope of $\overline{N_1N_\alpha}$. Then, the linear function that describes the cable $\overline{N_1N_\alpha}$ is given by

$$y = a\left(x - x_{N_1}\right) + y_{N_1},$$

where $a \geq e_1$. Then the coordinates of N_α are

$$\begin{cases} x_{N_\alpha} = x_{N_1} + \dfrac{\hat{d}}{\sqrt{1+a^2}}, \\ y_{N_\alpha} = y_{N_1} + \dfrac{a\hat{d}}{\sqrt{1+a^2}}. \end{cases}$$

For any point $S = (x, 0)$ on the EFL, the three possible candidates for $d(S)$ are

$$d_1(x) = \sqrt{(x - x_{N_1})^2 + y_{N_1}^2/\varepsilon^2}, \tag{8}$$

$$d_2(x) = \frac{\mid a(x - x_{N_1}) + y_{N_1} \mid}{\sqrt{a^2+\varepsilon^2}}, \tag{9}$$

and

$$d_3(x) = \sqrt{(x - x_{N_\alpha})^2 + y_{N_\alpha}^2/\varepsilon^2}. \tag{10}$$

Let $S_1, S_2 \in \mathcal{D}$ be the epicenters of the two ellipses (whose eccentricity is e) such that $\overline{N_1N_\alpha}$ is the tangent at N_1 and N_α to the two ellipses, respectively (see Fig. 6. Note that such two ellipses always exist under the assumptions made in (1) that the distance between N_1 and N_2 is significantly smaller the length of the EFL). We obtain that

$$x_{S_1} = x_{N_1} + \frac{a}{\varepsilon^2} y_{N_1}, \tag{11}$$

and

$$x_{S_2} = x_{N_\alpha} + \frac{a}{\varepsilon^2} y_{N_\alpha}. \tag{12}$$

There are four cases for the CBP:

1) When $x_{S_1} \geq -\hat{\mathcal{D}}/2$ and $x_{S_2} \leq \hat{\mathcal{D}}/2$:

$$\begin{aligned} P(\text{break}) = &\int_{-\hat{\mathcal{D}}/2}^{x_{S_1}} q(d_1(x))p(x)dx \\ &+ \int_{x_{S_1}}^{x_{S_2}} q(d_2(x))p(x)dx + \int_{x_{S_2}}^{\hat{\mathcal{D}}/2} q(d_3(x))p(x)dx, \end{aligned}$$

2) When $x_{S_1} \geq -\hat{\mathcal{D}}/2$ and $x_{S_2} > \hat{\mathcal{D}}/2$:

$$P(\text{break}) = \int_{-\hat{\mathcal{D}}/2}^{x_{S_1}} q(d_1(x))p(x)dx + \int_{x_{S_1}}^{\hat{\mathcal{D}}/2} q(d_2(x))p(x)dx,$$

3) When $x_{S_1} < -\hat{\mathcal{D}}/2$ and $x_{S_2} \leq \hat{\mathcal{D}}/2$:

$$P(\text{break}) = \int_{-\hat{\mathcal{D}}/2}^{x_{S_2}} q(d_2(x))p(x)dx + \int_{x_{S_2}}^{\hat{\mathcal{D}}/2} q(d_3(x))p(x)dx,$$

4) When $x_{S_1} < -\hat{\mathcal{D}}/2$ and $x_{S_2} > \hat{\mathcal{D}}/2$:

$$P(\text{break}) = \int_{-\hat{\mathcal{D}}/2}^{\hat{\mathcal{D}}/2} q(d_2(x))p(x)dx,$$

where $d_1(x)$ - $d_3(x)$ are given by (8)-(10), and x_{S_1}, x_{S_2} are given by (11), (12), respectively.

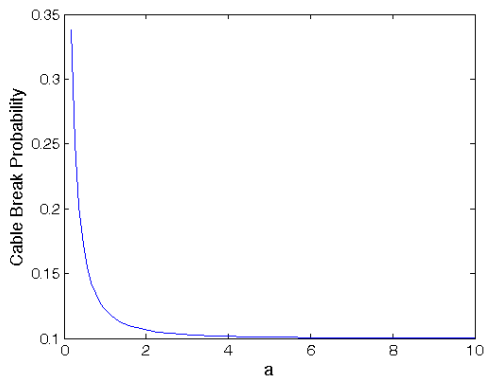

Fig. 7. CBP versus a for the rotated straight lines.

We again use the parameters of Table I to illustrate how the parameter a affects the CBP. The numerical results are shown in Fig. 7. We observe the CBP decreases as the parameter a increases, and since a is monotone in α, the CBP is a decreasing function of α, when $0^\circ < \alpha \leq 90^\circ$. The CBP reaches its minimum when the cable is laid perpendicular to the EFL. This can be explained intuitively by observing that if we position the cable perpendicular to the EFL, we minimize the number of points on the cable that may be affected by an earthquake. This insight is useful in designing cable shapes with low break probabilities.

V. Three Connected Segments

The straight line cable costs the least, but its CBP is high. In this section, we consider a cable shape called Three Connected Segments (TCS), where we restrict the set of candidate cable functions to a shape described by Fig. 3. Each cable we consider consists of three segments: $\overline{N_1D}$, $\overline{DE}$ and $\overline{EN_2}$. The middle segment $\overline{DE}$ always passes through the point C, where C is the crossing point of $\overline{N_1N_2}$ and the EFL. The coordinates of C are $(-e_2/e_1, 0)$. Let the angle between the middle segment $\overline{DE}$ and the y-axis be θ. Let m be the slope of $\overline{DE}$. Then the linear function that describes $\overline{DE}$ is given by

$$y = m(x + \frac{e_2}{e_1}),$$

where $m = \tan(90^\circ - \theta)$ and $m \geq e_1$. We define the parameter Δ_T to be equal to length of the middle segment $\overline{DE}$. There is a one-to-one correspondence between the value of Δ_T and the set of cable functions under TCS. For each value of Δ_T, we ensure that the triangles N_1CD and N_2CE are two similar triangles. Thus, we have

$$\frac{|N_1C|}{|CN_2|} = \frac{|DC|}{|CE|} = \frac{|N_1D|}{|EN_2|}.$$

Denote the slope of $\overline{N_1D}$ and $\overline{N_2E}$ by k. We obtain the expression of k, which is

$$k(\Delta_T, m) = e_1 + \frac{(m - e_1)\Delta_T}{\Delta_T - (x_{N_2} - x_{N_1})\sqrt{1 + m^2}}.$$

For any point $S = (x, 0)$ on the EFL, we have

$$d(S) = \min_{M \in \mathcal{L}} d(M, S).$$

We take the derivative of $d(M, S)$ (of the variable x_M), and let it be equal to 0. Then we obtain that there are five possible candidates for $d(S)$, which are

$$d_{T1}(S) = d_{T1}(x) = \sqrt{(x - x_{N_1})^2 + y_{N_1}^2/\varepsilon^2}, \tag{13}$$

$$d_{T2}(S) = d_{T2}(x, \Delta_T, m) = \frac{|\, kx - kx_{N_1} + y_{N_1} \,|}{\sqrt{k^2 + \varepsilon^2}}, \tag{14}$$

$$d_{T3}(S) = d_{T3}(x, m) = \frac{|\, mx + me_2/e_1 \,|}{\sqrt{m^2 + \varepsilon^2}}, \tag{15}$$

$$d_{T4}(S) = d_{T4}(x, \Delta_T, m) = \frac{|\, kx - kx_{N_2} + y_{N_2} \,|}{\sqrt{k^2 + \varepsilon^2}}, \tag{16}$$

and

$$d_{T5}(S) = d_{T5}(x) = \sqrt{(x - x_{N_2})^2 + y_{N_2}^2/\varepsilon^2}. \tag{17}$$

The five candidates for $d(S)$ have the following geometric meanings:

1) $d_{T1}(S)$: the equivalent distance from S to N_1;
2) $d_{T2}(S)$: the equivalent distance from S to $\overleftrightarrow{DN_1}$;
3) $d_{T3}(S)$: the equivalent distance from S to $\overleftrightarrow{DE}$;
4) $d_{T4}(S)$: the equivalent distance from S to $\overleftrightarrow{EN_2}$;
5) $d_{T5}(S)$: the equivalent distance from S to N_2.

We see that only the functions $d_{T2}(x, \Delta_T, m)$ and $d_{T4}(x, \Delta_T, m)$ depend on Δ_T. This implies that, for a given value of m, the value of Δ_T can dictate which is the smallest distance among the five candidates for $d(S)$. Therefore, according to the value of Δ_T, the problem is further divided into two scenarios as shown in Fig. 8. Next, we find the interval of Δ_T for each of the two scenarios.

Let $S_{T5} \in \overline{AC}$ be the epicenter of the ellipse (whose eccentricity is e) such that $\overline{DE}$ is the tangent to the ellipse and N_1 is on the ellipse. Similarly, let $S_{T6} \in \overline{CB}$ be the epicenter of another ellipse (whose eccentricity is e) such that $\overline{DE}$ is the tangent to the ellipse and N_2 is on the ellipse. Then, we have $d(S_{T5}) = d_{T1}(S_{T5}) = d_{T3}(S_{T5})$ and

$d(S_{T6}) = d_{T3}(S_{T6}) = d_{T5}(S_{T6})$. The x-coordinates of S_{T5} and S_{T6} are

$$x_{S_{T5}}(m) = x_{N_1} + \left(m^2 - \sqrt{(m^2+\varepsilon^2)(m^2-e_1^2)}\right)\frac{y_{N_1}}{e_1\varepsilon^2}, \tag{18}$$

and

$$x_{S_{T6}}(m) = x_{N_2} + \left(m^2 - \sqrt{(m^2+\varepsilon^2)(m^2-e_1^2)}\right)\frac{y_{N_2}}{e_1\varepsilon^2}, \tag{19}$$

respectively. There is a value of Δ_T such that $\overline{N_1D}$ is the tangent at N_1 to the ellipse with the epicenter S_{T5}, and $\overline{N_2E}$ is the tangent at N_2 to the ellipse with epicenter S_{T6}, respectively. We obtain this boundary value of Δ_T, which is

$$\Delta_{T\_bound}(m) = \frac{\sqrt{1+m^2}(x_{N_2}-x_{N_1})(m^2-e_1^2-\sqrt{(m^2+\varepsilon^2)(m^2-e_1^2)})}{m^2-e_1m-\sqrt{(m^2+\varepsilon^2)(m^2-e_1^2)}}. \tag{20}$$

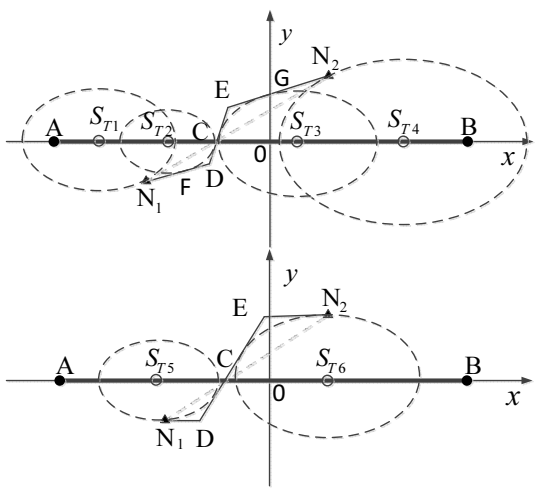

Fig. 8. Two scenarios of the cables under TCS.

The scenario described in Fig. 8(a) corresponds to the case $0 \le \Delta_T \le \Delta_{T\_bound}(m)$. For this scenario, let $S_{T1} \in \overline{AC}$ be the epicenter of the ellipse (whose eccentricity is e) such that $\overline{N_1D}$ is the tangent at N_1 to the ellipse. Similarly, let $S_{T4} \in \overline{CB}$ be the epicenter of another ellipse (whose eccentricity is e) such that $\overline{N_2E}$ is the tangent at N_2 to the ellipse. Then, we have $d(S_{T1}) = d_{T1}(S_{T1}) = d_{T2}(S_{T1})$ and $d(S_{T4}) = d_{T4}(S_{T4}) = d_{T5}(S_{T4})$. Let $S_{T2} \in \overline{S_{T1}C}$ be the epicenter of the ellipse (whose eccentricity is e) such that $\overline{DE}$ is the tangent to the ellipse and $\overline{N_1D}$ is the tangent at F to the ellipse, where $F \in \overline{N_1D}$. Similarly, let $S_{T3} \in \overline{CS_{T4}}$ be the epicenter of another ellipse (whose eccentricity is e) such that $\overline{DE}$ is the tangent to the ellipse and $\overline{N_2E}$ is the tangent at G to the ellipse, where $G \in \overline{N_2E}$. Then, we have $d(S_{T2}) = d_{T2}(S_{T2}) = d_{T3}(S_{T2})$ and $d(S_{T3}) = d_{T3}(S_{T3}) = d_{T4}(S_{T3})$. The x-coordinates of these four points are

$$x_{S_{T1}}(\Delta_T, m) = x_{N_1} + ky_{N_1}/\varepsilon^2, \tag{21}$$

$$x_{S_{T2}}(\Delta_T, m) = \frac{(kx_{N_1}-y_{N_1})\sqrt{m^2+\varepsilon^2}+me_2\sqrt{k^2+\varepsilon^2}/e_1}{k\sqrt{m^2+\varepsilon^2}-m\sqrt{k^2+\varepsilon^2}}, \tag{22}$$

$$x_{S_{T3}}(\Delta_T, m) = \frac{(kx_{N_2}-y_{N_2})\sqrt{m^2+\varepsilon^2}+me_2\sqrt{k^2+\varepsilon^2}/e_1}{k\sqrt{m^2+\varepsilon^2}-m\sqrt{k^2+\varepsilon^2}}, \tag{23}$$

and

$$x_{S_{T4}}(\Delta_T, m) = x_{N_2} + ky_{N_2}/\varepsilon^2, \tag{24}$$

respectively. In this case, we have

$$d(S) = \begin{cases} d_{T1}(S), & S \in \overline{AS_{T1}}, \\ d_{T2}(S), & S \in \overline{S_{T1}S_{T2}}, \\ d_{T3}(S), & S \in \overline{S_{T2}S_{T3}}, \\ d_{T4}(S), & S \in \overline{S_{T3}S_{T4}}, \\ d_{T5}(S), & S \in \overline{S_{T4}B}. \end{cases}$$

The CBP is obtained by

$$\begin{aligned} P(\text{break}) = &\int_{-\hat{\mathcal{D}}/2}^{x_{S_{T1}}} q(d_{T1}(x))p(x)dx \\ &+ \int_{x_{S_{T1}}}^{x_{S_{T2}}} q(d_{T2}(x,\Delta_T,m))p(x)dx \\ &+ \int_{x_{S_{T2}}}^{x_{S_{T3}}} q(d_{T3}(x,m))p(x)dx \\ &+ \int_{x_{S_{T3}}}^{x_{S_{T4}}} q(d_{T4}(x,\Delta_T,m))p(x)dx \\ &+ \int_{x_{S_{T4}}}^{\hat{\mathcal{D}}/2} q(d_{T5}(x))p(x)dx, \end{aligned} \tag{25}$$

where $d_{T1}(x)$ - $d_{T5}(x)$ are given by (13) - (17), and $x_{S_{T1}}$ - $x_{S_{T4}}$ are given by (21) - (24).

Proposition 1. *The function $P(\text{break})$ given by (25) is monotonically non-increasing in Δ_T for $\Delta_T \in (0, \Delta_{T\_bound}(m))$.*

Proof: See the Appendix. ■

The scenario described in Fig. 8(b) corresponds to the case $\Delta_T \ge \Delta_{T\_bound}(m)$. For this scenario, we have

$$d(S) = \begin{cases} d_{T1}(S), & S \in \overline{AS_{T5}}, \\ d_{T3}(S), & S \in \overline{S_{T5}S_{T6}}, \\ d_{T5}(S), & S \in \overline{S_{T6}B}. \end{cases}$$

The CBP is obtained by

$$\begin{aligned} P(\text{break}) = &\int_{-\hat{\mathcal{D}}/2}^{x_{S_{T5}}} q(d_{T1}(x))p(x)dx \\ &+ \int_{x_{S_{T5}}}^{x_{S_{T6}}} q(d_{T3}(x,m))p(x)dx + \int_{x_{S_{T6}}}^{\hat{\mathcal{D}}/2} q(d_{T5}(x))p(x)dx, \end{aligned} \tag{26}$$

where $d_{T1}(x)$, $d_{T3}(x,m)$, $d_{T5}(x)$ are given by (13), (15), (17), and $x_{S_{T5}}$, $x_{S_{T6}}$ are given by (18), (19), respectively. The CBP given by (26) is independent of Δ_T.

In the first scenario, the CBP given by (25) does not increase as Δ_T increases. In the second scenario, the CBP given by (26) is independent of Δ_T. Hence, for a given value of m, the CBP is monotonically non-increasing in Δ_T reaching its minimum for $\Delta_T \geq \Delta_{T\_boud}(m)$.

Intuitively, when increasing the length of the middle segment, the length of the entire cable increases. The cost of the cable is obtained by

$$C(\Delta_T, m) = c\left(x_{N_2} - x_{N_1} - \frac{\Delta_T}{\sqrt{1+m^2}}\right)\sqrt{1+k^2} + c\Delta_T, \tag{27}$$

which is monotonically increasing in Δ_T.

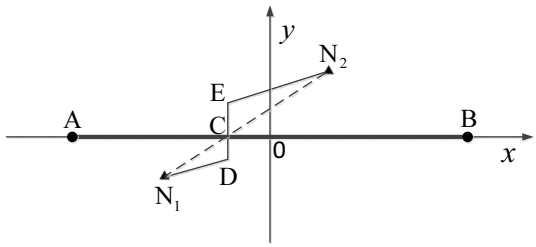

Fig. 9. A special case of TCS ($\theta = 0°$).

Fig. 9 illustrates a special case of TCS, where the middle cable segment is positioned vertically to the EFL. In this case, $\theta = 0°$ and $m = \infty$.

In summary, we list the procedure of our method to generate the Pareto front under TCS shape as follows.

- **Input**: Two endpoints of the EFL, A and B; two points to be connected with a cable, N_1, N_2; cost of the cable per unit length, c; eccentricity e of the elliptical isoseismals; probability density function of location of epicenters; CCB function;
- For each $\theta \in [0, 90° - \arctan e_1]$,
  - For each $\Delta_T > 0$,,
    - Calculate CBP by (25) or (26);
    - Calculate the cable cost by (27);
- Generate Pareto front curves by each pair of the CBP and the cable cost corresponding to the same Δ_T.

To illustrate the monotonicity of the CBP, we use (7) as the explicit CCB function and the spatial distribution of epicenters. We again use the parameters of Table I, and verify the expressions (25) and (26) by simulations which are shown in Fig. 10. For each of the curves, the CBP decreases and reaches a plateau, as Δ_T increases. The analytical results are always within the confidence intervals of the simulation results.

Having established the monotonicity of both the CBP and the cable cost functions, we generate the Pareto front (see Fig. 11) for these two objectives of the cables under TCS using the parameters of Table I. In each of the curves the angle is fixed as indicated. Then the curves in the figure are obtained by varying the length of the middle segment for each curve. The vertical dashed lines correspond to a range of costs for which the CBP

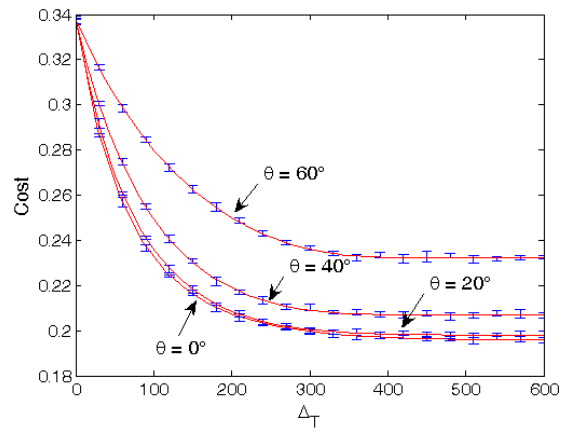

Fig. 10. CBP versus Δ_T for the cables under TCS.

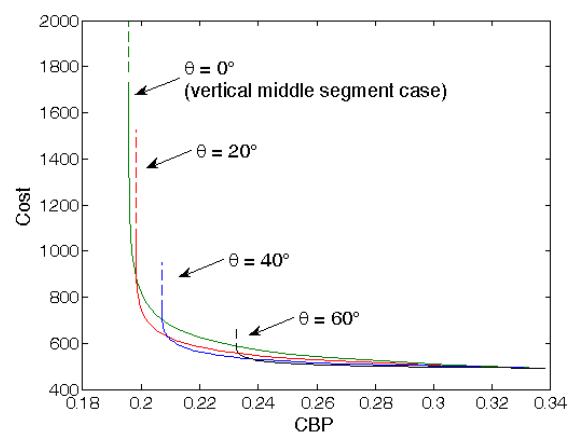

Fig. 11. Pareto Front for CBP and Cost of the cables under TCS.

does not change, and therefore they do not belong to the Pareto front curves. With the Pareto front, we also have solutions for the optimization problems of minimizing cost subject to a constraint on the CBP and of minimizing CBP subject to a constraint on the cable cost. In Fig. 11, all the curves meet at the point where the middle segment is of length equal to zero. Then they all represent a straight line between N_1 and N_2. At that point we obtain the minimal cost to be equal to 492.7038 and the CBP to be equal to 0.3379. This is the case of the straight line cable, which we studied in Section IV-A. We observe that for every θ value there is a minimum CBP that can be reached by extending the length of the middle cable. Then further reductions in CBP are not achievable because the further extension is already out of the "danger zone". We also observe that lower θ values give lower minimum CBP values, where the case $\theta = 0$ gives the lowest minimum CBP value. This is consistent with the examples presented in Section IV, and the intuitive explanation that the vertical line has minimal exposure to the "danger zone". It is also consistent with practice used by cable surveyors [55].

VI. Hook with Right Angles

Based on the insight gained from the cable rotation exercise in Section IV, to reduce the CBP, another option is to position the cable perpendicular to the EFL to minimize the number of points on the cable that may be affected by an earthquake, and continue in a straight line to move away from the fault as fast as possible until reaching a safe ground on the other side. Then, lay the cable in parallel to the EFL for a sufficiently long distance and finally return to the destination. The effectiveness of this approach depends on the length it is laid on safe ground in parallel to the EFL. Recall that we assume without loss of generality that N_1 is closer to the EFL than N_2. Otherwise, this HRA cables shape will start at N_2 and end at N_1.

This gives rise to another three-segment cable shape called Hook with Right Angles (HRA), where we restrict the set of candidate cable functions to a shape described by Fig. 4. Each cable we consider consists of three segments: $\overline{N_1D}$, $\overline{DE}$ and $\overline{EN_2}$. We position the first cable segment $\overline{N_1D}$ perpendicular to the EFL. The crossing point of $\overline{N_1D}$ and the EFL is denoted by C. We position the middle segment $\overline{DE}$ parallel to the EFL and position the last cable segment $\overline{EN_2}$ perpendicular to $\overline{DE}$. The shape of the entire cable resembles a hook with three segments and two right angles. We define the parameter Δ_H to be equal to the length of the cable segment $\overline{EN_2}$. There is a one-to-one correspondence between the value of Δ_H and the set of cable functions under HRA.

For any point $S = (x, 0)$ on the EFL, we have

$$d(S) = \min_{M \in \mathcal{L}} d(M, S).$$

We take the derivative of $d(M, S)$ (of the variable x_M), and let it be equal to 0. Then we obtain that there are three possible candidates for $d(S)$, which are

$$d_{H1}(S) = d_{H1}(x) = |x - x_{N_1}|, \tag{28}$$

$$d_{H2}(S) = d_{H2}(\Delta_H) = (y_{N_2} + \Delta_H)/\varepsilon, \tag{29}$$

and

$$d_{H3}(S) = d_{H3}(x) = \sqrt{(x - x_{N_2})^2 + y_{N_2}^2/\varepsilon^2}. \tag{30}$$

The three candidates for $d(S)$ have the following geometric meanings:

1) $d_{H1}(S)$: the equivalent distance from S to C;
2) $d_{H2}(S)$: the equivalent distance from S to $\overleftrightarrow{DE}$;
3) $d_{H3}(S)$: the equivalent distance from S to N_2.

Let F be orthogonal projection of N_2 on the EFL. When $|CF| \leq |FN_2|/\varepsilon$, for any $S \in \overline{CF}$, the equivalent distance $d(S)$ is always $d_{H1}(S)$. In this scenario, the CBP is not a function of Δ_H. Increasing Δ_H does not help in reducing the CBP. However, in the scenario that $|CF| > |FN_2|/\varepsilon$, increasing Δ_H reduces the CBP. Therefore, in the following, we only consider the scenario that $|CF| > |FN_2|/\varepsilon$, which is in particular

$$x_{N_2} - x_{N_1} > y_{N_2}/\varepsilon. \tag{31}$$

Equation (31) ensures the effectiveness of HRA, and as mentioned above, it is related to having sufficient length parallel to the EFL in "safe ground".

With a fixed value of Δ_H, the function $d_{H2}(\Delta_H)$ is constant for any $S \in \mathcal{D}$. And we see that only $d_{H2}(\Delta_H)$ depends on Δ_H. This implies that the value of Δ_H can dictate which is the smallest distance among the three candidates for $d(S)$. Therefore, according to the value of Δ_H, the problem is further divided into two scenarios as shown in Fig. 12.

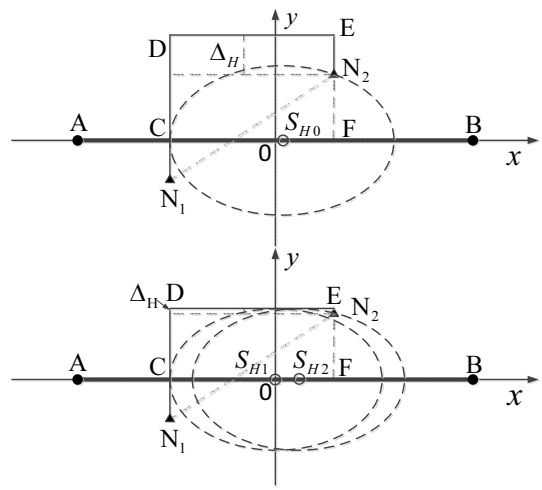

Fig. 12. Two scenarios of the cables under HRA.

Let $S_{H0} \in \overline{CF}$ be the epicenter of the ellipse (whose eccentricity is e) such that the points C and N_2 are on the ellipse. Thus, we have $d_{H1}(S_{H0}) = d_{H3}(S_{H0})$. The x-coordinate of S_{H0} is

$$x_{S_{H0}} = \frac{x_{N_2}^2 - x_{N_1}^2 + y_{N_2}^2/\varepsilon^2}{2(x_{N_2} - x_{N_1})}. \tag{32}$$

The scenario described in Fig. 12(a) corresponds to the case $d_{H2}(\Delta_H) \geq d_{H1}(S_{H0}) = d_{H3}(S_{H0})$. The range of Δ_H for this scenario is

$$\Delta_H \geq \frac{\varepsilon(x_{N_2} - x_{N_1})^2 + y_{N_2}^2/\varepsilon}{2(x_{N_2} - x_{N_1})} - y_{N_2}.$$

In this case, we have

$$d(S) = \begin{cases} d_{H1}(S), & S \in \overline{AS_{H0}}, \\ d_{H3}(S), & S \in \overline{S_{H0}B}. \end{cases}$$

The CBP is obtained by

$$\begin{aligned} P(\text{break}) = &\int_{-\hat{\mathcal{D}}/2}^{x_{S_{H0}}} q(d_{H1}(x))p(x)dx \\ &+ \int_{x_{S_{H0}}}^{\hat{\mathcal{D}}/2} q(d_{H3}(x))p(x)dx, \end{aligned} \tag{33}$$

where $d_{H1}(x)$, $d_{H3}(x)$ are given by (28), (30), and $x_{S_{H0}}$ is given by (32). The CBP in (33) is independent of Δ_H.

The scenario described in Fig. 12(b) corresponds to the case $d_{H2}(\Delta_H) < d_{H1}(S_{H0}) = d_{H3}(S_{H0})$. The range of Δ_H for

this scenario is

$$0 \leq \Delta_H < \frac{\varepsilon(x_{N_2} - x_{N_1})^2 + y_{N_2}^2/\varepsilon}{2(x_{N_2} - x_{N_1})} - y_{N_2}.$$

For this scenario, let $S_{H1} \in \overline{CS_{H0}}$ be the epicenter of the ellipse (whose eccentricity is e) such that the point C is on the ellipse and $\overline{DE}$ is the tangent to the ellipse. Similarly, let $S_{H2} \in \overline{S_{H0}F}$ be the epicenter of another ellipse (whose eccentricity is e) such that the point N_2 is on the ellipse and $\overline{DE}$ is the tangent to the ellipse. Thus, we have $d_{H1}(S_{H1}) = d_{H2}(\Delta_H) = d_{H3}(S_{H2})$. The x-coordinates of S_{H1} and S_{H2} are

$$x_{S_{H1}}(\Delta_H) = x_{N_1} + (y_{N_2} + \Delta_H)/\varepsilon, \tag{34}$$

and

$$x_{S_{H2}}(\Delta_H) = x_{N_2} - \frac{1}{\varepsilon}\sqrt{\Delta_H^2 + 2y_{N_2}\Delta_H}, \tag{35}$$

respectively. In this case, we have

$$d(S) = \begin{cases} d_{H1}(S), & S \in \overline{AS_{H1}}, \\ d_{H2}(\Delta_H), & S \in \overline{S_{H1}S_{H2}}, \\ d_{H3}(S), & S \in \overline{S_{H2}B}. \end{cases}$$

The CBP is obtained by

$$P(\text{break}) = \int_{-\hat{\mathcal{D}}/2}^{x_{S_{H1}}} q(d_{H1}(x))p(x)dx + q(d_{H2}(\Delta_H)) \int_{x_{S_{H1}}}^{x_{S_{H2}}} p(x)dx + \int_{x_{S_{H2}}}^{\hat{\mathcal{D}}/2} q(d_{H3}(x))p(x)dx, \tag{36}$$

where $d_{H1}(x)$ - $d_{H3}(x)$ are given by (28) - (30), and $x_{S_{H1}}$, $x_{S_{H2}}$ are given by (34), (35).

Proposition 2. *The function $P(\text{break})$ given by (36) is monotonically non-increasing in Δ_H for*

$$\Delta_H \in \left(0, \frac{\varepsilon(x_{N_2} - x_{N_1})^2 + y_{N_2}^2/\varepsilon}{2(x_{N_2} - x_{N_1})} - y_{N_2}\right).$$

Proof: See the Appendix. ■

In the first scenario, the CBP given by (33) is independent of Δ_H. In the second scenario, the CBP given by (36) does not increase as Δ_H increases. Hence, for the entire range of Δ_H, the CBP is monotonically non-increasing in Δ_H reaching its minimum for

$$\Delta_H \geq \frac{\varepsilon(x_{N_2} - x_{N_1})^2 + y_{N_2}^2/\varepsilon}{2(x_{N_2} - x_{N_1})} - y_{N_2}.$$

The cost of a HRA cable is obtained by

$$C(\Delta_H) = c\left(y_{N_2} - y_{N_1} + x_{N_2} - x_{N_1} + 2\Delta_H\right), \tag{37}$$

which is monotonically increasing in Δ_H.

We also summarize the procedure of our method to generate the Pareto front under HRA shape as follows.

- **Input**: Two endpoints of the EFL, A and B; two points to be connected with a cable, N_1, N_2; cost of the cable per unit length, c; eccentricity e of the elliptical isoseismals; probability density function of location of epicenters; CCB function;
- For each $\Delta_H > 0$,
  - Calculate CBP by (33) or (36);
  - Calculate the cable cost by (37);
- Generate Pareto front curves by each pair of the CBP and the cable cost corresponding to the same Δ_H.

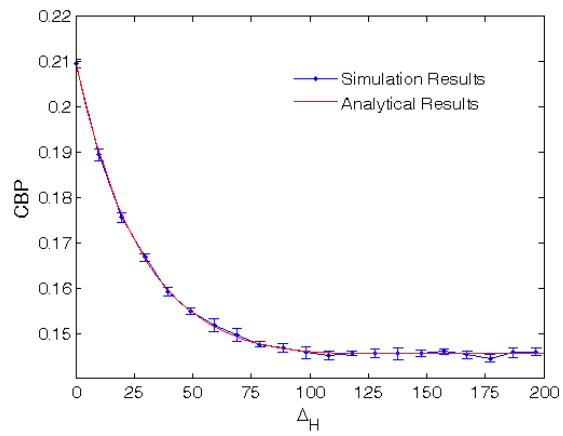

Fig. 13. CBP versus Δ_H for the cables under HRA.

To illustrate the monotonicity of the CBP, we use (7) as the explicit CCB function and the spatial distribution of epicenters. We again use the parameters of Table I and verify the expressions (33) and (36) by simulations which are shown in Fig. 13. Note that the parameters of Table I satisfy the condition of (31). The CBP decreases and reaches a plateau, as Δ_H increases. The analytical results are within the confidence intervals of the simulation results.

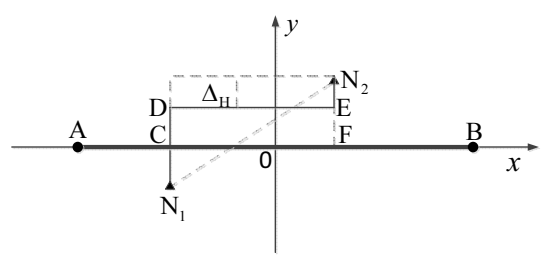

Fig. 14. A visual description of the special cases with negative Δ_H value.

Finally, we would like to discuss the special cases illustrated in Fig. 14, where the middle segment of a cable still has right angles with $\overleftrightarrow{N_1D}$ and $\overleftrightarrow{FN_2}$, but the cable does not have a hook shape, because its middle segment is between the EFL and N_2. For consistency with the previous Δ_H definition, we define Δ_H as taking negative values in such cases, and in particular, we consider the Δ_H values in the range $-|FN_2| \leq \Delta_H < 0$. In such cases, the cable cost does not vary with Δ_H, but the CBP increases as the middle segment approaches the EFL, and reaches its maximum value when $\Delta_H = -|FN_2|$. This

maximum value is obtained by

$$P(\text{break}) = \int_{-\hat{\mathcal{D}}/2}^{x_{N_1}} q\left(|x - x_{N_1}|\right) p(x)dx + q(0)\int_{x_{N_1}}^{x_{N_2}} p(x)dx + \int_{x_{N_2}}^{\hat{\mathcal{D}}/2} q\left(|x - x_{N_2}|\right) p(x)dx.$$

Using (7) and the parameters of Table I, we obtain the numerical value of this maximum CBP, which is 0.5495.

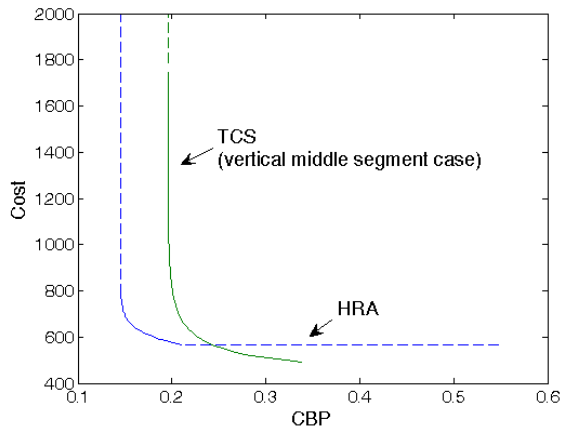

Fig. 15. Pareto Fronts for CBP and Cost of the cables under TCS and HRA.

Having established the monotonicity of both the CBP and the cable cost functions, we generate the Pareto front for these two objectives of the cables under HRA and compare it with the Pareto front of the cables under TCS (vertical middle segment case). The two Pareto fronts are shown in Fig. 15. The vertical dashed lines correspond to a range of costs for which the CBP does not change. The horizontal dashed line corresponds to a range of CBP for which the costs does not change. Therefore, the dashed lines do not belong to the Pareto front curves, based on the Pareto front definition, in which it is impossible to make one objective better off without making the other objective worse off. The Pareto front curves enable us to solve the optimization problems of minimizing cost subject to a constraint on the CBP and of minimizing CBP subject to a constraint on the cable cost, for cables under TCS and HRA. We observe that, under the condition of (31), HRA is applicable to scenarios with strict CBP requirements, while TCS is applicable to scenarios with limited budget. Having the two Pareto fronts together as shown in Fig. 15 enables the cable path planning in accordance with the design requirements.

VII. Conclusion

We have considered the problem of how to lay a single cable to connect two points across an EFL. We have formulated the problem as a multi-objective optimization on the plane that considers cable cost and CBP as two objectives. We have gained insight from the rotation exercise of a straight-line cable and further considered two important and meaningful sets of cable shape alternatives. For each set of alternatives, we have identified the key attributes which affect both the cable cost and the CBP. We have derived the expressions that have led to the Pareto fronts for the two objectives under TCS and HRA, which enable us to solve two single objective optimization problems of minimizing cost subject to a constraint on the CBP, and of minimizing CBP subject to a constraint on the cable cost.

Although our approach relies on a 2D simplification, it provides a step-stool for the more complex 3D multi-objective optimization problem, where the geography as well as the real earthquake effects are considered, and Pareto front solutions are derived.

Appendix

Proof of Proposition 1: We have

$$\begin{aligned}\frac{dP(\text{break})}{d\Delta_T} &= q(d_{T1}(x_{S_{T1}}))\frac{dx_{S_{T1}}}{d\Delta_T}p(x_{S_{T1}}) \\ &- q(d_{T2}(x_{S_{T1}}, \Delta_T, m))\frac{dx_{S_{T1}}}{d\Delta_T}p(x_{S_{T1}}) \\ &+ q(d_{T2}(x_{S_{T2}}, \Delta_T, m))\frac{dx_{S_{T2}}}{d\Delta_T}p(x_{S_{T2}}) \\ &- q(d_{T3}(x_{S_{T2}}, m))\frac{dx_{S_{T2}}}{d\Delta_T}p(x_{S_{T2}}) \\ &+ q(d_{T3}(x_{S_{T3}}, m))\frac{dx_{S_{T3}}}{d\Delta_T}p(x_{S_{T3}}) \\ &- q(d_{T4}(x_{S_{T3}}, \Delta_T, m))\frac{dx_{S_{T3}}}{d\Delta_T}p(x_{S_{T3}}) \\ &+ q(d_{T4}(x_{S_{T4}}, \Delta_T, m))\frac{dx_{S_{T4}}}{d\Delta_T}p(x_{S_{T4}}) \\ &- q(d_{T5}(x_{S_{T4}}))\frac{dx_{S_{T4}}}{d\Delta_T}p(x_{S_{T4}}) \\ &+ \int_{x_{S_{T1}}}^{x_{S_{T2}}} \frac{\partial q(d_{T2}(x, \Delta_T, m))}{\partial \Delta_T}p(x)dx \\ &+ \int_{x_{S_{T3}}}^{x_{S_{T4}}} \frac{\partial q(d_{T4}(x, \Delta_T, m))}{\partial \Delta_T}p(x)dx.\end{aligned}$$

In the scenario described in Fig. 8(a), we have

$$d_{T1}(x_{S_{T1}}) = d_{T2}(x_{S_{T1}}, \Delta_T, m),$$

$$d_{T2}(x_{S_{T2}}, \Delta_T, m) = d_{T3}(x_{S_{T2}}, m),$$

$$d_{T3}(x_{S_{T3}}, m) = d_{T4}(x_{S_{T3}}, \Delta_T, m),$$

and

$$d_{T4}(x_{S_{T4}}, \Delta_T, m) = d_{T5}(x_{S_{T4}}).$$

Thus, we have

$$\begin{aligned}
&\frac{dP(\text{break})}{d\Delta_T} \\
&= \int_{x_{S_{T1}}}^{x_{S_{T2}}} \frac{\partial q(d_{T2}(x,\Delta_T,m))}{\partial \Delta_T} p(x)dx \\
&\quad + \int_{x_{S_{T3}}}^{x_{S_{T4}}} \frac{\partial q(d_{T4}(x,\Delta_T,m))}{\partial \Delta_T} p(x)dx \\
&= \int_{x_{S_{T1}}}^{x_{S_{T2}}} q'(d_{T2}(x,\Delta_T,m)) \frac{\partial d_{T2}(x,\Delta_T,m)}{\partial \Delta_T} p(x)dx \\
&\quad + \int_{x_{S_{T3}}}^{x_{S_{T4}}} q'(d_{T4}(x,\Delta_T,m)) \frac{\partial d_{T4}(x,\Delta_T,m)}{\partial \Delta_T} p(x)dx.
\end{aligned}$$

Since $q(\cdot)$ is defined as a monotonically decreasing derivable function, we have $q'(d_{T2}(x,\Delta_T,m)) < 0$ and $q'(d_{T4}(x,\Delta_T,m)) < 0$. We further obtain that

$$\begin{aligned}
&\frac{\partial d_{T2}(x,\Delta_T,m)}{\partial \Delta_T} \\
&= \frac{\varepsilon^2 (x - x_{S_{T1}})(m - e_1)(x_{N_2} - x_{N_1})\sqrt{1+m^2}}{\left(\Delta_T - (x_{N_2} - x_{N_1})\sqrt{1+m^2}\right)^2 (k^2+\varepsilon^2)^{3/2}},
\end{aligned}$$

and

$$\begin{aligned}
&\frac{\partial d_{T4}(x,\Delta_T,m)}{\partial \Delta_T} \\
&= \frac{\varepsilon^2 (x_{S_{T4}} - x)(m - e_1)(x_{N_2} - x_{N_1})\sqrt{1+m^2}}{\left(\Delta_T - (x_{N_2} - x_{N_1})\sqrt{1+m^2}\right)^2 (k^2+\varepsilon^2)^{3/2}}.
\end{aligned}$$

Note that we defined that $m > e_1$. Thus, for $x \in (x_{S_{T1}}, x_{S_{T2}})$, we have

$$\frac{\partial d_{T2}(x,\Delta_T,m)}{\partial \Delta_T} > 0.$$

Similarly, for $x \in (x_{S_{T3}}, x_{S_{T4}})$, we have

$$\frac{\partial d_{T4}(x,\Delta_T,m)}{\partial \Delta_T} > 0.$$

Since $p(x) \geq 0$, we have

$$\frac{dP(\text{break})}{d\Delta_T} \leq 0.$$

Therefore, the function $P(\text{break})$ given by (25) is monotonically non-increasing in Δ_T for $\Delta_T \in (0, \Delta_{T\_bound}(m))$. ■

Proof of Proposition 2: We have

$$\begin{aligned}
&\frac{dP(\text{break})}{d\Delta_H} = q(d_{H1}(x_{S_{H1}})) \frac{dx_{S_{H1}}}{d\Delta_H} p(x_{S_{H1}}) \\
&+ q(d_{H2}(\Delta_H)) \left(\frac{dx_{S_{H2}}}{d\Delta_H} p(x_{S_{H2}}) - \frac{dx_{S_{H1}}}{d\Delta_H} p(x_{S_{H1}}) \right) \\
&+ \frac{dq(d_{H2}(\Delta_H))}{d\Delta_H} \int_{x_{S_{H1}}}^{x_{S_{H2}}} p(x)dx \\
&- q(d_{H3}(x_{S_{H2}})) \frac{dx_{S_{H2}}}{d\Delta_H} p(x_{S_{H2}}).
\end{aligned}$$

In the scenario described in Fig. 12(b), we have $d_{H1}(x_{S_{H1}}) = d_{H2}(\Delta_H) = d_{H3}(x_{S_{H2}})$. Thus, we have

$$\begin{aligned}
\frac{dP(\text{break})}{d\Delta_H} &= \frac{dq(d_{H2}(\Delta_H))}{d\Delta_H} \int_{x_{S_{H1}}}^{x_{S_{H2}}} p(x)dx \\
&= \frac{1}{\varepsilon} q'(d_{H2}(\Delta_H)) \int_{x_{S_{H1}}}^{x_{S_{H2}}} p(x)dx.
\end{aligned}$$

Since $q(\cdot)$ is defined as a monotonically decreasing derivable function, we have $q'(d_{H2}(\Delta_H)) < 0$. Furthermore, $\int_{x_{S_{H1}}}^{x_{S_{H2}}} p(x)dx \geq 0$. Thus we have

$$\frac{dP(\text{break})}{d\Delta_H} \leq 0.$$

Therefore, the function $P(\text{break})$ given by (36) is monotonically non-increasing in Δ_H for

$$\Delta_H \in \left(0, \frac{\varepsilon(x_{N_2} - x_{N_1})^2 + y_{N_2}^2/\varepsilon}{2(x_{N_2} - x_{N_1})} - y_{N_2}\right).$$

■

References

[1] MakaiPlan, "Submarine cable planning software." [Online]. Available: http://www.makai.com/cable-software/makaiplan/

[2] M. J. O'Rourke and X. Liu, "Response of buried pipelines subject to earthquake effects," *MCEER Technical Reports*, 1999. [Online]. Available: http://hdl.handle.net/10477/588

[3] USGS, "Significant earthquakes of the world, 1987," Mar. 2010. [Online]. Available: http://earthquake.usgs.gov/earthquakes/eqarchives/significant/sig_1987.php

[4] TeleGeography, "Earthquake highlights Asian dependency on submarine cables," Jan. 2007. [Online]. Available: http://www.telegeography.com/press/press-releases/2007/01/08/earthquake-highlights-asian-dependency-on-submarine-cables/index.html

[5] C. Barras, "Why the Mediterranean is the Achilles' heel of the web," Jan. 2009. [Online]. Available: http://www.newscientist.com/article/dn16394

[6] USGS, "Magnitude 9.0 - near the east coast of honshu, japan," Mar. 2011. [Online]. Available: http://earthquake.usgs.gov/earthquakes/eqinthenews/2011/usc0001xgp/usc0001xgp.php

[7] Y. Wang and S.-K. Au, "Spatial distribution of water supply reliability and critical links of water supply to crucial water consumers under an earthquake," *Reliability Engineering & System Safety*, vol. 94, no. 2, pp. 534–541, 2009.

[8] Y. Wang, S.-K. Au, and Q. Fu, "Seismic risk assessment and mitigation of water supply systems," *Earthquake Spectra*, vol. 26, no. 1, pp. 257–274, 2010.

[9] Y. Wang and T. D. O'Rourke, *Seismic performance evaluation of water supply systems*. Buffalo, NY: Multidisciplinary Center for Earthquake Engineering Research, 2008.

[10] W. W. Chen, B.-J. Shih, Y.-C. Chen, J.-H. Hung, and H. H. Hwang, "Seismic response of natural gas and water pipelines in the ji-ji earthquake," *Soil Dynamics and Earthquake Engineering*, vol. 22, no. 9, pp. 1209–1214, 2002.

[11] H. Hwang, Y.-H. Chiu, W.-Y. Chen, and B.-J. Shih, "Analysis of damage to steel gas pipelines caused by ground shaking effects during the chi-chi, taiwan, earthquake," *Earthquake spectra*, vol. 20, no. 4, pp. 1095–1110, 2004.

[12] S. Wang, L. Hong, M. Ouyang, J. Zhang, and X. Chen, "Vulnerability analysis of interdependent infrastructure systems under edge attack strategies," *Safety science*, vol. 51, no. 1, pp. 328–337, 2013.

[13] H. F. Zohra, B. Mahmouda, and D. Luc, "Vulnerability assessment of water supply network," *Energy Procedia*, vol. 18, pp. 772–783, 2012.

[14] K. Poljanšek, F. Bono, and E. Gutiérrez, "Seismic risk assessment of interdependent critical infrastructure systems: the case of european gas and electricity networks," *Earthquake engineering & structural dynamics*, vol. 41, no. 1, pp. 61–79, 2012.

[15] M. F. Habib, M. Tornatore, F. Dikbiyik, and B. Mukherjee, "Disaster survivability in optical communication networks," *Computer Communications*, vol. 36, no. 6, pp. 630 – 644, 2013.

[16] H. Saito, "Analysis of geometric disaster evaluation model for physical networks," *IEEE/ACM Trans. Netw*, vol. PP, no. 99, pp. 1–1, 2014.

[17] ——, "Spatial design of physical network robust against earthquakes," *J. Lightw. Technol*, vol. 33, no. 2, pp. 443–458, Jan. 2015.

[18] X. Wang, X. Jiang, and A. Pattavina, "Assessing network vulnerability under probabilistic region failure model," in *Proc. 12th IEEE Int. Conf. High Performance Switching and Routing (HPSR 2011)*,, Cartagena, Spain, Jul. 2011, pp. 164–170.

[19] J. Liu, X. Jiang, H. Nishiyama, and N. Kato, "Reliability assessment for wireless mesh networks under probabilistic region failure model," *IEEE Trans. Veh. Technol.*, vol. 60, no. 5, pp. 2253–2264, Jun. 2011.

[20] S. Neumayer and E. Modiano, "Network reliability with geographically correlated failures," in *Proc. IEEE INFOCOM 2010*, San Diego, CA, USA, Mar. 2010, pp. 1–9.

[21] S. Neumayer, G. Zussman, R. Cohen, and E. Modiano, "Assessing the impact of geographically correlated network failures," in *Proc. IEEE MILCOM 2008*, San Diego, CA, USA, Nov. 2008, pp. 1–6.

[22] ——, "Assessing the vulnerability of the fiber infrastructure to disasters," *IEEE/ACM Trans. Netw.*, vol. 19, no. 6, pp. 1610–1623, Dec. 2011.

[23] P. Agarwal, A. Efrat, S. Ganjugunte, D. Hay, S. Sankararaman, and G. Zussman, "Network vulnerability to single, multiple, and probabilistic physical attacks," in *Proc. IEEE MILCOM 2010*, San Jose, CA, USA, Oct. 2010, pp. 1824–1829.

[24] ——, "The resilience of WDM networks to probabilistic geographical failures," in *Proc. IEEE INFOCOM 2011*, Shanghai, China, Apr. 2011, pp. 1521–1529.

[25] S. Neumayer and E. Modiano, "Network reliability under random circular cuts," in *Proc. IEEE GLOBECOM 2011*, Houston, Texas, USA, Dec. 2011, pp. 1–6.

[26] ——, "Assessing the effect of geographically correlated failures on interconnected power-communication networks," in *Proc. IEEE Int. Conf. Smart Grid Communications (SmartGridComm) 2013*, Oct. 2013, pp. 366–371.

[27] S. Neumayer, A. Efrat, and E. Modiano, "Geographic max-flow and min-cut under a circular disk failure model," *Computer Networks*, vol. 77, no. 0, pp. 117 – 127, 2015.

[28] Y. Kobayashi and K. Otsuki, "Max-flow min-cut theorem and faster algorithms in a circular disk failure model," in *Proc. IEEE INFOCOM 2014*, Apr. 2014, pp. 1635–1643.

[29] W. Wu, B. Moran, J. H. Manton, and M. Zukerman., "Topology design of undersea cables considering survivability under major disasters," in *International Conference on Advanced Information Networking and Applications Workshops 2009*, Bradford, UK, May 2009, pp. 1154–1159.

[30] C. Cao, M. Zukerman, W. Wu, J. H. Manton, and B. Moran, "Survivable topology design of submarine networks," *J. Lightw. Technol*, vol. 31, no. 5, pp. 715–730, Mar. 2013.

[31] R. L. Kovach, *Early Earthquakes of the Americas*. Cambridge University Press, 2004.

[32] D. J. Dowrick and D. A. Rhoades, "Attenuation of modified mercalli intensity in new zealand earthquakes," *Bulletin of The New Zealand Society for Earthquake Engineering*, vol. 32, no. 2, pp. 55–89, 1999.

[33] B. K. Rastogi and H. K. Gupta, *Dams and Earthquakes*. Elsevier Science, 1975.

[34] Y.-X. Hu, S.-C. Liu, and W. Dong, *Earthquake engineering*. CRC Press, 1996.

[35] J. Koyama, *The complex faulting process of earthquakes*. Springer Science & Business Media, 2013, vol. 16.

[36] A. K. Tang, *Izmit (Kocaeli), Turkey, Earthquake of August 17, 1999 Including Duzce Earthquake of November 12, 1999: Lifeline Performance*. ASCE Publications, 2000, vol. 17.

[37] S. L. Kramer, *Geotechnical earthquake engineering*. Upper Saddle River, NJ: Prentice Hall, 1996, vol. 80.

[38] N. Ghazisaidi, M. Scheutzow, and M. Maier, "Survivability analysis of next-generation passive optical networks and fiber-wireless access networks," *IEEE Trans. Reliab.*, vol. 60, no. 2, pp. 479–492, June 2011.

[39] I. Ouveysi and A. Wirth, "On design of a survivable network architecture for dynamic routing: Optimal solution strategy and an efficient heuristic," *Eur. J. Oper. Res.*, vol. 117, no. 1, pp. 30–44, 1999.

[40] I. Ouveysi, A. Wirth, A. Yeh, and O. Oguz, "Large scale linear programs and heuristics for the design of survivable telecommunication networks," *Ann. Oper. Res.*, vol. 124, pp. 285–293, 2003.

[41] Y.-K. Lin, "Reliability of a stochastic-flow network with unreliable branches nodes, under budget constraints," *IEEE Trans. Reliab.*, vol. 53, no. 3, pp. 381–387, Sep. 2004.

[42] Y.-K. Lin and C.-T. Yeh, "Evaluation of optimal network reliability under components-assignments subject to a transmission budget," *IEEE Trans. Reliab.*, vol. 59, no. 3, pp. 539–550, Sep. 2010.

[43] E. Modiano and A. Narula-Tam, "Survivable routing of logical topologies in WDM networks," in *Proc. IEEE INFOCOM 2001*, Anchorage, Alaska, USA, 2001, pp. 348–357.

[44] W.-C. Yeh, Y.-C. Lin, Y. Chung, and M. Chih, "A particle swarm optimization approach based on monte carlo simulation for solving the complex network reliability problem," *IEEE Trans. Reliab.*, vol. 59, no. 1, pp. 212–221, Mar. 2010.

[45] K. S. Ho and K. W. Cheung, "Generalized survivable network," *IEEE/ACM Trans. Netw*, vol. 15, no. 4, pp. 750–760, Aug. 2007.

[46] O. Wasem, "An algorithm for designing rings for survivable fiber networks," *IEEE Trans. Reliab.*, vol. 40, no. 4, pp. 428–432, Oct. 1991.

[47] A. Narula-Tam, E. Modiano, and A. Brzezinski, "Physical topology design for survivable routing of logical rings in WDM-based networks," *IEEE J. Sel. Areas Commun.*, vol. 22, no. 8, pp. 1525–1538, Oct. 2004.

[48] D. K. Lynch, "San andreas fault." [Online]. Available: http://www.sanandreasfault.org

[49] G. Einziger, B. Fellman, and Y. Kassner, "Independent counter estimation buckets," in *Proc. IEEE INFOCOM 2015*, Hong Kong, PRC, 2015.

[50] P. Hick, "CAIDA Anonymized 2013 Internet Trace, equinix-sanjose 2013-1-17 13: 55 UTC, Direction B."

[51] W. Smith, "Reducing the subjectivity in Modified Mercalli intensity analysis: drawing isoseismals," in *Proceedings of 2007 New Zealand Society for Earthquake Engineering Conference (NZSEE)*, Wellington, New Zealand, 2007, pp. 1–7.

[52] C. Cornell, "Engineering seismic risk analysis," *Bulletin of the Seismological Society of America*, vol. 58, no. 5, pp. 1583–1606, 1968.

[53] J. W. Baker, "Introduction to probabilistic seismic hazard analysis. white paper," Stanford University, Tech. Rep., 2015.

[54] M. D. Petersen, M. P. Moschetti, P. M. Powers, C. S. Mueller, K. M. Haller, A. D. Frankel, Y. Zeng, S. Rezaeian, S. C. Harmsen, O. S. Boyd *et al.*, "Documentation for the 2014 update of the united states national seismic hazard maps," US Geological Survey, Tech. Rep., 2014.

[55] E. Tahchi, private communication, Nov. 2014.

[56] TeleGeography, "Submarine cable map 2014," 2014. [Online]. Available: http://submarine-cable-map-2014.telegeography.com/

[57] R. R. Youngs and K. J. Coppersmith, "Implications of fault slip rates and earthquake recurrence models to probabilistic seismic hazard estimates," *Bulletin of the Seismological society of America*, vol. 75, no. 4, pp. 939–964, 1985.

[58] P. Cosentino, V. Ficarra, and D. Luzio, "Truncated exponential frequency-magnitude relationship in earthquake statistics," *Bulletin of the Seismological Society of America*, vol. 67, no. 6, pp. 1615–1623, 1977.

[59] G. Purcaur and D. Zorilescu, "A magnitude-frequency relation for the lognormal distribution of earthquake magnitude," *Pure Appl. Geophys.*, vol. 87, pp. 43–53, 1971.

[60] S.-S. Jeon and T. D. O'Rourke, "Northridge earthquake effects on pipelines and residential buildings," *Bulletin of the Seismological Society of America*, vol. 95, no. 1, pp. 294–318, 2005.

Cong Cao received the B.Eng. degree in Information Engineering with First Class Honors from the City University of Hong Kong, Hong Kong SAR, China, in 2010. He is currently working toward the Ph.D. degree in electrical engineering at the same university. His current research is in the area of telecommunication network topology design for disaster survivability.

Zengfu Wang received the B.Sc. degree in applied mathematics, the M.Sc. degree in control theory and control engineering, the Ph.D. degree in control science and engineering from Northwestern Polytechnical University, Xian, in 2005, 2008, and 2013 respectively. He is currently a Postdoctoral Fellow with City University of Hong Kong, HK, and a lecturer with Northwestern Polytechnical University. His research interests include path planning, discrete optimization and information fusion.

Moshe Zukerman (M'87–SM'91–F'07) received the B.Sc. degree in industrial engineering and management and the M.Sc. degree in operations research from the Technion – Israel Institute of Technology, Haifa, Israel, and the Ph.D. degree in engineering from University of California, Los Angeles, in 1985. He was an independent Consultant with the IRI Corporation and a Postdoctoral Fellow with the University of California, Los Angeles, in 1985–1986. In 1986–1997, he was with Telstra Research Laboratories (TRL), first as a Research Engineer and, in 1988–1997, as a Project Leader. He also taught and supervised graduate students at Monash University in 1990–2001. During 1997-2008, he was with The University of Melbourne, Victoria, Australia. In 2008 he joined City University of Hong Kong as a Chair Professor of Information Engineering, and a team leader. He has over 300 publications in scientific journals and conference proceedings. He has served on various editorial boards such as Computer Networks, IEEE Communications Magazine, IEEE Journal of Selected Ares in Communications, IEEE/ACM Transactions on Networking and the International Journal of Communication Systems.

Jonathan Manton holds a distinguished Chair at the University of Melbourne with the title Future Generation Professor. He is also an Adjunct Professor in the Mathematical Sciences Institute at the Australian National University. He received his Bachelor of Science (mathematics) and Bachelor of Engineering (electrical) degrees in 1995 and his Ph.D. degree in 1998, all from the University of Melbourne, Australia. From 1998 to 2004, he was with the Department of Electrical and Electronic Engineering at the University of Melbourne. During that time, he held a Postdoctoral Research Fellowship then subsequently a Queen Elizabeth II Fellowship, both from the Australian Research Council. In 2005 he became a full Professor in the Department of Information Engineering, Research School of Information Sciences and Engineering (RSISE) at the Australian National University. From July 2006 till May 2008, he was on secondment to the Australian Research Council as Executive Director, Mathematics, Information and Communication Sciences. Manton's traditional research interests range from pure mathematics (e.g. commutative algebra, algebraic geometry, differential geometry) to engineering (e.g. signal processing, wireless communications). He has recently served as a Guest Editor for a special issue on Differential Geometry in Signal Processing, he has been an Associate Editor for IEEE TRANSACTIONS ON SIGNAL PROCESSING and Committee Member for IEEE Signal Processing for Communications (SPCOM) Technical Committee.

Alain Bensoussan is Ashbel Smith Professor and the Director of ICDRiA (International Center for Decision and Risk Analysis) at the University of Texas at Dallas. He is also Chair Professor of Risk and Decision Analysis at the City University Hong Kong. He is Professor Emeritus at the University Paris Dauphine. Professor Bensoussan served as President of National Institute for Research in Computer Science and Control (INRIA) from 1984 to 1996; President of the French Space Agency (CNES) from 1996 to 2003; and Chairman of the European Space Agency (ESA) Council from 1999 to 2002. He was World Class University Distinguished Professor at Ajou University, from 2010 to 2013. He is a member of the French Academy of Sciences, French Academy of Technology, Academia Europae, and International Academy of Astronautics. His distinctions include AMS Fellow, IEEE Fellow, SIAM Fellow, Von Humboldt award, and the NASA public service medal. Professor Bensoussan is a decorated Officer of Legion d'Honneur, Commandeur Ordre National du Merite and Officer Bundes Verdienst Kreuz. He has an extensive research background in stochastic control, risk analysis and inventory control. He has published 13 books and more than 400 papers in journals and conference proceedings. He develops a comprehensive approach to Risk Analysis, to apprehend technical and socio-economic risks simultaneously. He has experience in aerospace and information technology industries. His main current interests concern the energy sector, real options, revenue management and mean field control.

Yu Wang is an associate professor of geotechnical engineering at City University of Hong Kong. He obtained his Ph.D. degree from Cornell University, USA, in 2006. His recent research efforts have focused on geotechnical uncertainty, risk and reliability (e.g., probabilistic characterization of soil properties, reliability-based design, probabilistic slope stability analysis), soil-structure interaction (e.g., responses of buried utility pipelines to ground displacement induced by seismic strong motions or urban underground construction activities such as tunneling), and seismic risk assessment of critical civil infrastructure systems (e.g. water supply systems and submarine telecommunication cables). His research has earned several international recognitions, including the inaugural Wilson Tang best paper award in Singapore in 2012. He was the President of American Society of Civil Engineers (ASCE) - Hong Kong Section in 2012 - 2013. He is also a member of several international Technical Committees (TCs), including an ASCE Geo-Institute TC on Risk and two TCs on Risk and In-Situ Testing, respectively, under the International Society of Soil Mechanics and Geotechnical Engineering. Dr Wang has authored/co-authored over 80 technical publications, including about 40 journal papers and one book published by John Wiley & Sons.